

A CHEVRON NOTCHED WEDGE LOADED DOUBLE CANTILEVER BEAM TEST METHOD TO MEASURE THE INITIATION AND ARREST FRACTURE TOUGHNESS OF SEMIBRITTLE MATERIALS WITH SMALL SPECIMENS—G. R. Odette, M. Y. He, and M. L. Hribernik
(University of California, Santa Barbara)

OBJECTIVE

The objective of this work was to develop a chevron-notched, wedge-loaded, double-cantilever beam fracture toughness test method, based on a comprehensive finite element analysis that was used to select an effective specimen geometry and to quantify the stress intensity factor. This new test method was used to measure the initiation and arrest toughness of both TiAl at ambient temperature and cleavage oriented single crystal Fe over a wide range of temperatures.

SUMMARY

Our goal was to design a specimen and test procedure that allowed the initiation and arrest of a crack in very small cleavage oriented iron single crystals (< 10 mm). This was accomplished by incorporating iron single crystal slices into composite specimens. The test method described here is based on a chevron-notched, wedge-loaded, double-cantilever beam specimen. Conceptually, slow insertion of the wedge, to load the beam arms, gradually increases the crack mouth opening displacement (Δ), and the corresponding stress intensity factor (SIF), K_I , up to K_{Ic} , thus initiating a propagating cleavage crack. However, due to the combination the wedge loading a double-cantilevered beam and chevron geometry, the K_I decreases very rapidly with increasing depth (a/W), and the crack arrests at a SIF $K_I = K_{Ia}$, after a short pop-in jump. Thus the crack can be grown in a series of short, and relatively stable, jumps. The initiation and arrest-re-initiation depths can be seen on the fracture surface.

Implementation of this concept required an extensive finite element (FE) analysis, both to select an effective specimen geometry and to quantify the stress intensity factor in terms of its relation to the measured test parameters. In addition to the effects of varying specimen geometry, the FE analysis was used to examine the effects such plastic deformation and slanting of the crack front. Both monolithic and composite 'sandwich' type specimens were modeled, where the effects of the modulus difference between the oriented single crystal Fe and the polycrystalline steel was investigated in the latter case. The K_I was also found to vary along the crack front, with a broad minimum in the center and local maxima at the side-corners of the of chevron wedge. This so-called 'chevron-wedge-beam' (CWB) test method was evaluated with tests on TiAl, that showed a consistent K_{Ic} and K_{Ia} are obtained by assuming that initiation occurs at the chevron corners and arrest near the center of the crack front. The average $K_{Ic} \approx 7.1 \pm 1 \text{ MPa}\sqrt{\text{m}}$ measured with the CWB test method is consistent with the previous measurements of the toughness of fatigue pre-cracked TiAl bend bars with $K_{Ic} \approx 8 \pm 1 \text{ MPa}\sqrt{\text{m}}$ and the results of notched double anvil compression specimen tests with $K_{Ip} \approx 7.1 \pm 0.7 \text{ MPa}\sqrt{\text{m}}$. Note the CWB test method can also be applied to other brittle and semi-brittle materials.

PROGRESS AND STATUS

Introduction

The new test method described here was specifically developed to provide a way to measure the initiation and arrest toughness, K_{Ic} and K_{Ia} , of small cleavage oriented iron single crystals. Cylindrical rods of unalloyed iron single crystals, slightly less than 1 cm in diameter and 5-6 cm in length, were cut to within 15° of the specified axial orientation. Oriented crystal sections were EDM sectioned and trimmed to ≈ 2 mm thick rectangular slices that were then diffusion bonded to low alloy steel arms that acted to transmit loads and release elastic strain energy. The CWB test method resembles the procedure in ASTM Standard E 1304-97 [1]. However, the CWB test method developed in this study differs from the one in the Standard in three major ways. First, the CWB specimen is much smaller than the E 1304-97 configuration, due to the limited sizes and

amounts of available oriented Fe single crystals. Second, the CWB test method loading is carried out under crack mouth opening displacement (Δ) control, leading to much higher crack growth stability, compared to the grip loading method used in the ASTM Standard. Third, at least in the case of the Fe single crystal measurements, the CWB tests involve composite specimens. Thus an extensive set of FE calculations was required to select the CWB specimen geometry and to quantify the stress intensity factor as a function of the specimen size, Δ , the elastic modulus (E), and the crack lengths at initiation (a_i) and arrest (a_a).

The Finite Element Model

The first set of calculations was carried out for a monolithic CWB specimen under fully elastic loading conditions, as characterized by the elastic modulus (E). The chevron-notched wedge specimen geometry is specified by the dimensions in the sketch of the specimen shown in Fig. 1a. These dimensions include the specimen thickness (B), width (W), the beam height (2h), the depth of the initial chevron point (a_0) relative to the loading line, the crack depths, a_i for initiation, and a_a for arrest. The Mode I SIF, K_I , can be specified by the Δ , or the load (P), using the following standard relations:

$$K_I = Y_d E \Delta / \sqrt{B} \quad (1)$$

and

$$K_I = Y_p P / (B \sqrt{a}) \quad (2)$$

The non-dimensional Y_d and Y_p factors are functions of the overall CWB specimen geometry that was selected based on the FE analysis. The Y_d and Y_p represent non-dimensional forms of the SIF that are quantified in this report.

The commercial finite element code ABAQUS/standard was used for the analysis. Twenty-node quadratic isoparametric brick elements were employed to model one quarter of the specimen. A quarter-point crack tip element served to model the inverse square root stress singularity at the crack front. A typical finite element mesh, which contains 4350 elements and 24024 nodes, is shown in Fig. 1b. A half-specimen mesh was also used to evaluate the effects of variations in the crack depth along the crack front.

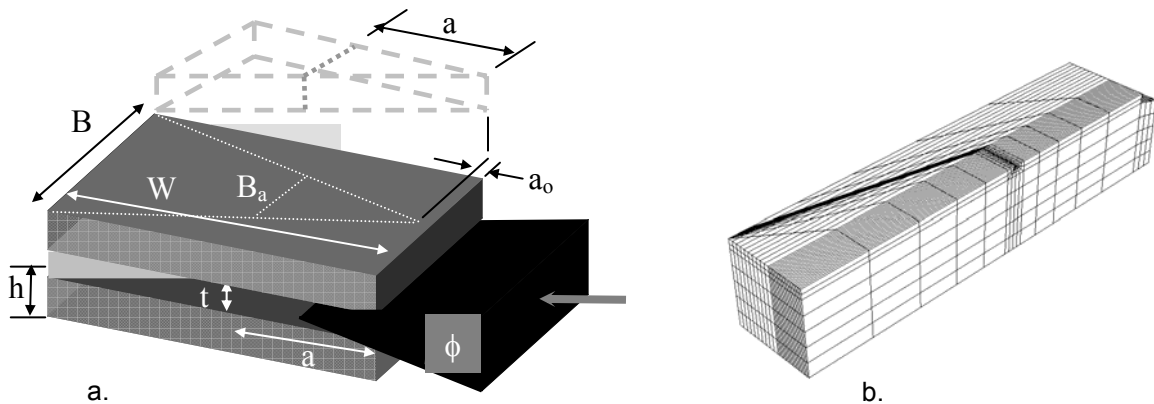


Fig. 1. a) The CWB specimen showing the key dimensions (not to scale). b) The quarter section the mesh used in the FE model.

The values of J along the crack front were calculated by the domain integral method. Five contours were used, and the scatter of J for the various contours was less than 1% due to the finely focused crack front mesh. The SIF were obtained from J as

$$K_I = \sqrt{\left(\frac{EJ}{1-\nu^2}\right)} \quad (3)$$

The 3D finite element analysis gave accurate results for SIF, even for the relatively coarse five layer mesh [2]. Based on a careful convergence study, meshes of 9, 14, 30, and 50 layers were used. The 9 layer model was sufficiently accurate to calculate the average SIF. The 30 and 50 layer meshes were used to calculate the SIF at the corner and for the slanted crack front, where higher accuracy was necessary.

The elastic calculations were complemented by elastic plastic modeling of the monolithic specimen using constitutive laws in the form:

$$\frac{\varepsilon_e}{\varepsilon_y} = \left(\frac{\sigma_e}{\sigma_y}\right)^n \quad \text{for } \sigma_e > \sigma_y \quad (4)$$

Where σ_e is effective stress defined by the stress deviator S_{ij} as:

$$\sigma_e = \left(\frac{3}{2} S_{ij} S_{ij}\right)^{1/2} \quad (5)$$

ε_e is the effective strain defined as:

$$\varepsilon_e = \left(\frac{2}{3} \varepsilon_{ij} \varepsilon_{ij}\right)^{1/2} \quad (6)$$

The results reported here are for a yield stress, $\sigma_y = 500$ MPa, and a Ramberg-Osgood power law hardening exponent of $n = 10$.

Elastic FE calculations were also carried out for a composite sandwich specimen containing a single crystal chevron shaped slice with modulus E_c that differs from E for the CWB arms. In this case the thickness (t) of the single crystal also slightly influences the SIF.

Finite Element Results

Monolithic Specimens

A main purpose of the FE analysis was to determine the SIF values as a function of crack depth, a/W . Several specimen geometries were selected as candidates for the calculations and specimen design. The two W/B were 1.45 and 2.0, consistent with the recommendations of ASTM E 1304. For $W/B = 1.45$, FE calculations were carried out for three a_o/W of 0, 0.18, 0.3. For $W/B = 2$, FE calculations were carried out only for $a_o/W = 0$. The total beam height, including the Fe crystal slice, was fixed a $B/2$. The SIFs at the mid-plane of the crack front are shown in Fig. 2. Under load control (Fig. 2a), the critical crack length occurs at the CWB specimen's SIF minimum. However, the minimum occurs at $a/W = 0$ for $a_o/W = 0$, and increases continuously at larger crack depths, as illustrated in Fig. 2a. Increasing a_o/W ultimately results in a very shallow minimum, as shown in Fig. 2a to occur at $a_o/W = 0.3$. However, none of these geometries have a SIF versus a/W curve that would result in crack arrest under load control.

In contrast, under displacement controlled wedge crack mouth opening loading, the CWB specimen SIF rapidly decreases with the increasing a/W , as shown in Fig. 2b. The larger $W/B =$

2 produces a more rapid decreases, compared to the $W/B = 1.45$ case. It is also clear that $a_0/W = 0$ is desirable, since this geometry gives larger distances and a wider range of decreasing SIFs for crack initiation and arrest pop-in events. Thus $W/B = 2$ and $a_0/W = 0$ were selected for further modeling.

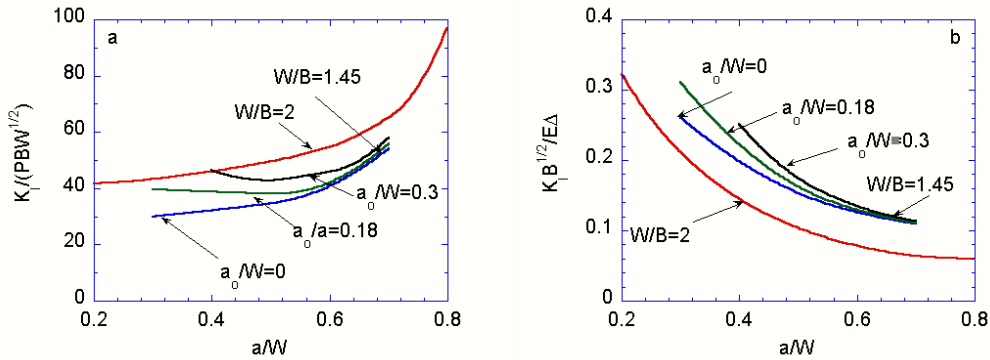


Fig. 2. a) The SIF (Y_p and Y_d) as a functions of crack length a/W , for various specimen geometries, normalized by P . b) The SIF (Y_p and Y_d) as a functions of crack length a/W , for various specimen geometries, normalized by Δ .

Three-dimensional effects along the chevron crack front as a function of x/B_a are very important. Here x is the distance from the center plane ($x = 0$) of the crack front in the thickness direction and B_a is the total crack front length at a crack depth of a . For, $a > a_0$ the crack front has two corners, where it intersects the edges of the chevron wedge at $x/B_a = \pm 0.5$. The corners lead to secondary stress concentrations and higher SIFs than at the crack front center at $x = 0$. The SIF distributions along the crack front are shown in Fig. 3a for $a/W = 0.5$ in terms of the $K_I(x/B_a)/K_I(0)$ ratio. The $K_I(x/B_a)/K_I(0)$ ratio is nearly constant for $x/B_a < 0.35$, but rapidly increases as x/B_a approaches 0.5. The $K_I(x/B_a)/K_I(0)$ ratio depends on a/W . Figure 3b shows the SIF as a function of a/W for both $x/B_a = 0$ and ≈ 0.5 . The $K_I(a/W)$ for $x/B_a \approx 0.5$ is about 30% higher than for $x/B_a \approx 0$. Note, the K values at $x/B_a \approx 0.5$, obtained from the domain integrals, are only estimates. A detailed discussion of the corner singularity effects can be found elsewhere [3].

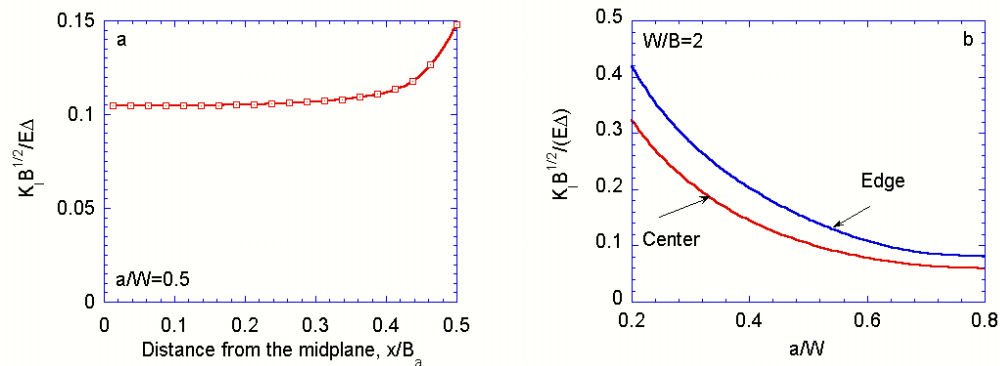


Fig. 3. a) The SIF distribution along the crack front for $a/W = 0.5$. b) The SIF functions for the crack center and edge.

Since crack initiation requires high stresses over a finite material dimension, the K_I values near $x/B_a \approx 0.5$ are believed to provide the best estimates of the effective SIF for crack initiation, K_{Ic} . Likewise, the lower SIF at $x/B_a = 0$ provides the best K_I estimate of the arrest K_{Ia} . These trends have been observed experimentally in the CWB tests on Fe single crystals, and are discussed further in the section on the calibration of the CWB test method.

The Effects of Slanted Crack Fronts

Figure 4 illustrates the effects of a slanted crack front, as characterized by a slant angle $\alpha > 0$ (see the insert in Fig. 4a), by plotting the SIF for x/B_a between ± 0.5 at $a/W = 0.5$. Figure 4a shows the SIF decreases continuously from a maximum at the acute angle of intersection of the crack front with the edge of the chevron with the shallowest depth, at $x/B_a = -0.5$, to a minimum at the corresponding obtuse angle with the largest depth, at $x/B_a = +0.5$. The effect of a slanted crack front increases with α , but only slightly between 10 and 14° . Figure 4b shows that the maximum to minimum SIF ratio, $K_I(-0.5)/K_I(0.5)$, increases with a/W . However, the K_I at the $x = 0$ crack front midplane, $K_I(0)$ is independent of α . The maximum $K_I(-0.5)$ is also relatively insensitive to crack slanting, increasing by only about 7% for α from 10 to 14° , compared to a unslanted, $\alpha = 0$, crack front. Thus the initiation toughness can be approximately evaluated from the unslanted ($\alpha = 0$) crack curve shown in Fig. 3b. The minimum $K_I(0.5)$ is about 80 to 90% of the SIF for the unslanted crack at $x/B_a = 0$. Thus, the arrest toughness K_{Ia} could be somewhat overestimated using the $x/B_a = 0$ curve in Fig. 3b. However crack slanting has little effect around $x/B_a = 0$ and the minimum SIF at $x/B_a = 0.5$ only bounds K_{Ia} . The fact that the arrest must occur over a significant length of the crack front provides an averaging effect that would mitigate any local minimum SIF effects of moderately slanted cracks on K_{Ia} . Thus it is also reasonable to use the lower $x/B_a = 0.0$ curve in Fig. 3b to assess K_{Ia} .

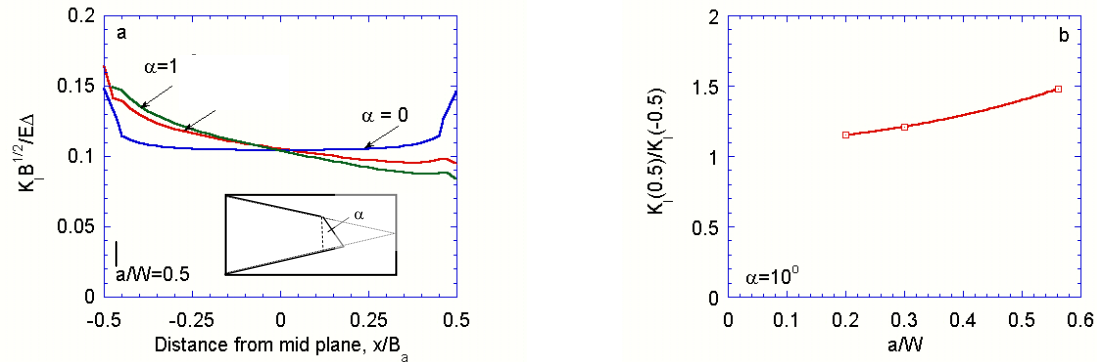


Fig. 4. Effects of slanting of the crack front on the SIF: a) For $a/W = 0.5$, and $\alpha = 0, 10^\circ$ and 14° . b) The ratio of SIF of short intersection to the long intersection for $\alpha = 10^\circ$.

The Effects of Plastic Deformation

Plastic deformation generally reduces the elastic crack tip energy release rate and the corresponding elastic SIF at a specified loading, as represented by Δ/B for the CWB test. Figure 5 plots the normalized SIF as a function of Δ/B for the constitutive law described previously, assuming a yield stress of $\sigma_y = 500$ MPa and a Ramberg-Osgood strain hardening exponent of $n = 10$. The curves are for $a/W = 0.2$ and 0.5 at various x/B_a points along the crack front. For fully elastic loading, the SIF is proportional to Δ , hence, K/Δ , is approximately independent of Δ . Figure 4a shows plasticity results in a small initial peak in the SIF for Δ/B between about 0 to 0.006, followed by significant decreases at higher loading. For example for $x/B_a = 0$, the SIF decreases by more than a factor of 2 between $\Delta/B = 0.01$ and 0.05, roughly scaling as $\sqrt[3]{(B/\Delta)}$. The small peak in the SIF slightly increases with larger x , but the variations with Δ/B are otherwise similar.

The effect of plasticity is much smaller for the deeper crack at $a/W = 0.5$. In this case, the small peak is shifted to larger Δ/B and plasticity induced reductions of SIF begin at about $\Delta/B > 0.02$, with a decrease between $\Delta/B = 0.01$ and 0.05 of about 25% at $x/B_a = 0$. In summary, effect plasticity depends on a/W , and is modest below about $0.01\Delta/B$ for $a/W = 0.2$ and $0.025\Delta/B$ for $a/W = 0.5$.

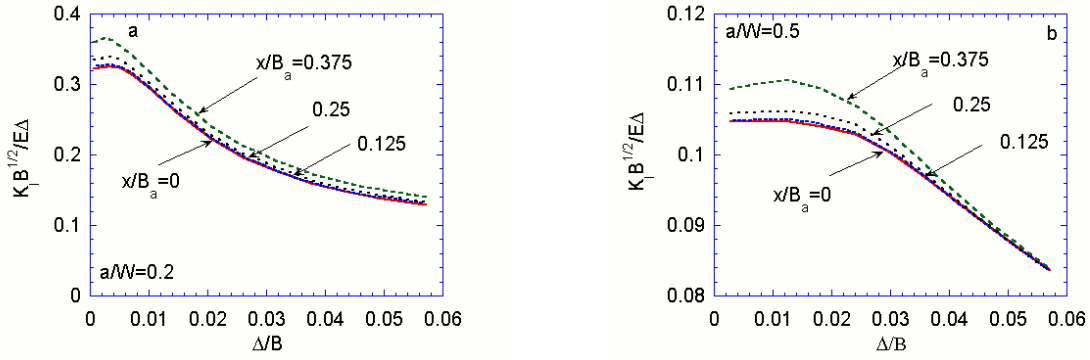


Fig. 5. Effects of the plastic deformation for a) $a/W = 0.2$ and b) $a/W = 0.5$.

Figure 6 plots the elastic plastic loading as a function of Δ/B in terms of the normalized crack tip opening displacement, δ/B , where δ is defined as the distance between the crack faces at the intercept of two symmetric 45° lines from the blunted crack tip. For small scale yielding (SSY) conditions δ is approximately linearly proportional to Δ , after the initial blunting transient, as observed for the $a/W = 0.5$ case. The curves for the shallower crack with $a/W = 0.3$ show a slight negative curvature that may indicate some deviations from SSY. Figure 7 shows the relation between δ , σ_y and J , expressed in terms of the standard coefficient, $d_n = \sigma_y \delta / J$; note, the subscript n indicates that d_n depends on the strain hardening behavior of the material. The d_n decreases rapidly with increasing Δ/B during the initial blunting transient and plateaus at a value of $d_n \approx 0.54$ for $a/W \approx 0.3$ to 0.6 , in good agreement with the previous results obtained by O'Dowd and Shih [4]. The d_n for the shallower $a/W = 0.2$ crack falls systematically lower by an increment of about 0.05.

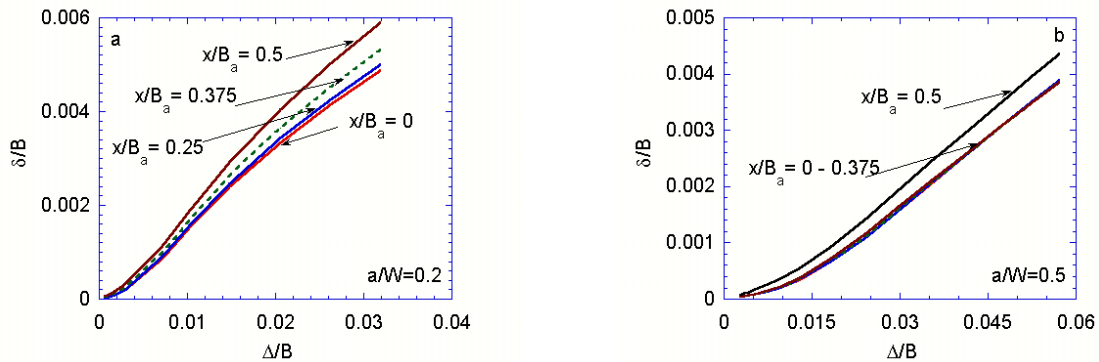


Fig. 6. The normalized δ/B as a functions of Δ/B for a) $a/W = 0.2$ and b) $a/W = 0.5$.

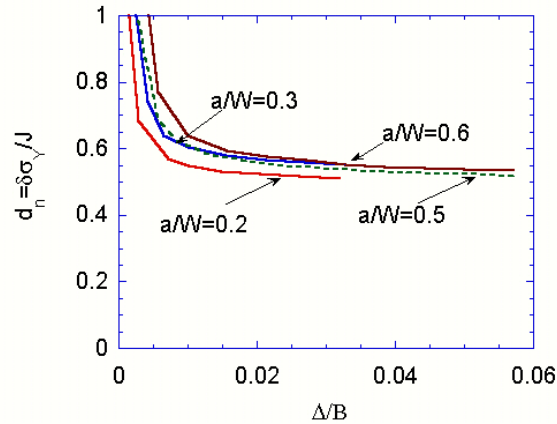


Fig. 7. The $d_n = \delta\sigma_y/J$ coefficient as a function of Δ/B for various a/W .

These results suggest that elastic plastic fracture mechanics can be used to analyze CWB test data, at least slightly beyond the elastic limit. Note, however, we have not carried out a detailed assessment of the crack tip fields for this geometry, including as they are influenced by the combination of plasticity and other potentially significant effects such as T-fields and variations along the crack front. There are likely differences between these fields and classical SSY fields that could be significant in interpreting the K_{Ic} and K_{Ia} measurements from the CWB test, especially as they might relate to more conventional SSY test geometries. It should also be noted that there is local plasticity (plastic zone formation) even when the overall cracked specimen is in the globally elastic loading regime, where the loading can be fully characterized by K_I . Further, in the case of semi-brittle cleavage fracture of single crystal iron, the local plasticity is associated with discrete dislocation slip traces, rather than quasi-homogeneous-continuum plastic zones.

Sandwich CWB Specimens

The high cost of iron single crystal and relatively small size of the oriented single crystal slices requires that they be incorporated in a composite specimen as shown in Fig. 1. The initial scoping studies confirmed that the basic geometry CWB of $W/B = 2$, $h/B = 0.5$ and $a_0/W = 0$ provides a large range of K_I over a/W distances sufficient for pop-in arrest events. The CWB specimens were fabricated by diffusion bonding an oriented single crystal slice to two adjoining low alloy steel arms to form a rectangular three-layer sandwich with a square cross section. This sandwich was then (electro-discharge machined) EDM in from the sides to form the chevron shaped iron single crystal wedge. A shallow 30° notch was also EDM in the arms at the tip of the chevron to provide mating surfaces for the wedge that produce uniform loading along the crack front. The effective loading point for the wedge induced displacements was taken at the $a_0/W = 0$ location in the FE calculations. A shallow $\approx 150 \mu\text{m}$ round notch was EDM into pointed end of the chevron to promote the first crack initiation event and to avoid interference between the single crystal and wedge. The first pop-in event was used to condition the CWB specimen with a sharp pre-crack at $a/W > 0$. A 1 mm half round notch was EDM on the back of the specimen to mate with a pin on the test fixture to provided precise specimen alignment, and unrestricted rotation of the beam arms. Knife edges were also EDM on the chevron tip end of the specimen for mounting a clip gauge to continuously measure Δ . Evaluation of the stresses in the plastic zone showed that the single crystal thickness of $t = 1 \text{ mm}$ was sufficient to avoid high interface stresses that might lead to debonding of the iron crystal from the beam arms. The overall dimensions of the CWB specimens were about 8mm wide by 4mm thick by 4 mm high.

The FE analysis was extended to treat the modulus difference of single crystal Fe section, taken as 130 GPa for the [100] direction, and the low alloy steel arms, taken as 200 GPa. The normalized SIF at the mid-plane as a function of crack length is given in Fig. 5a. The result for the monolithic material is also included for comparison, showing a difference approximately 5-10 % between the two cases. This is consistent with the relatively small difference between the volume weighted average modulus of the composite CWB specimen and that for the low alloy steel.

CWB Test Procedure and Evaluation

Evaluation of the CWB tests was performed on monolithic TiAl, first using a small table-top fixture, where the wedge was driven by a high resolution micrometer head. Previous tests on fatigue pre-cracked specimens on this same material measured an average $K_{Ic} \approx 8 \pm 1 \text{ MPa}\sqrt{\text{m}}$ [6]. A total of 30 CWB benchtop tests on TiAl gave an average $K_{Ic} = 7.2 \pm 1.3 \text{ MPa}\sqrt{\text{m}}$, and an average $K_{Ia} = 3.7 \pm 0.5 \text{ MPa}\sqrt{\text{m}}$ [5]. The results are shown in Fig. 8. Figure 8a shows the evaluation for based K_I averaged along the crack front for the sandwich specimen. The K_{Ic} appear to depend on a/W in this case, while the K_{Ia} do not. Figure 8b shows the corresponding TiAl toughness evaluation, assuming initiation occurs at the $K_I = K_{Ic}$ at $x/B_a = \pm 0.5$ (the edge), while arrest occurs at $K_I = K_{Ic}$ at $x/B_a = 0$ (near the center). Using the latter assumption, both K_{Ic} and K_{Ia} are independent of a/W .

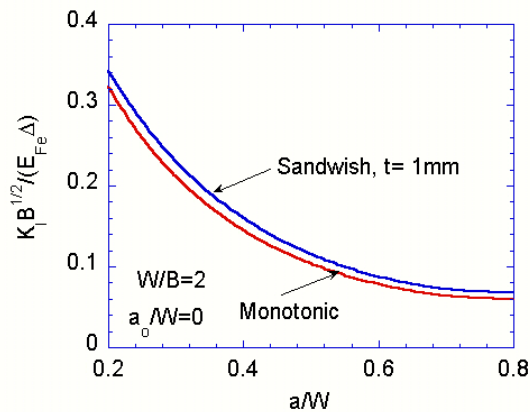


Fig. 8. a) Normalized SIF $x/B_a = 0$ as a function of crack length a/W for the monolithic and sandwich specimens.

However, the micrometer wedge fixture was intended only for the initial scoping studies and was far too compliant for actual single crystal testing and was limited to a maximum load of about 400 N. Thus a robust, low compliance crack mouth opening displacement fixture was designed and built for use with a MTS servohydraulic actuator to drive the wedge at a specified rate, typically about $1 \mu\text{m/s}$, corresponding to a stress intensity loading rate of about $0.25 \pm 0.15 \text{ MPa}\sqrt{\text{m/s}}$. The Δ was measured by a clip gage mounted on knife-edges on the outside of the beams. The wedge was stopped immediately after the rapid load drop that accompanied crack initiation and arrest. Crack initiation was also monitored with an acoustic emission detector. The initiation (a_i) and arrest (a_a) depths were easily observed on the fracture surfaces.

The loading fixture and instrumentation described above provided reliable and repeatable results. The TiAl data from a final test procedure calibration are shown in Figs. 9 and 10. Twelve tests gave an average of $K_I = 6.9 \pm 0.7 \text{ MPa}\sqrt{\text{m}}$ and $K_{Ia} = 3.7 \pm 0.5 \text{ MPa}\sqrt{\text{m}}$ [5]. The overall average of $K_{Ic} \approx 7.1 \pm 1 \text{ MPa}\sqrt{\text{m}}$ for all 42 TiAl tests is reasonably consistent with previous measurements with fatigue pre-cracked bend bars of $8 \pm 1 \text{ MPa}\sqrt{\text{m}}$ and the results of compression anvil notched

beam tests of $K_{Ic} \approx 7.1 \pm 0.7 \text{ MPa}\sqrt{\text{m}}$ [5,7]. The arrest toughness in the latter case was $K_{Ia} \approx 2.8 \pm 1.4 \text{ MPa}\sqrt{\text{m}}$ [5,7].

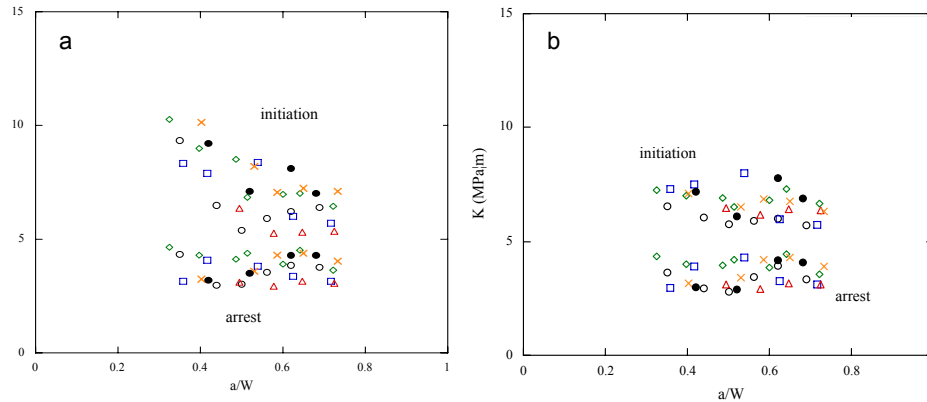


Fig. 9. a) The TiAl K_{Ic} and K_{Ia} values from the table top chevron-wedge technique showing a dependence on crack length (a/W) based on the average K_I . b) The TiAl K_{Ic} and K_{Ia} assuming that initiation is controlled by $K_I(a_i/B_a = \pm 0.5)$ and arrest is controlled by $K_I(a_a/B_a = 0)$, where both are independent of a/W .

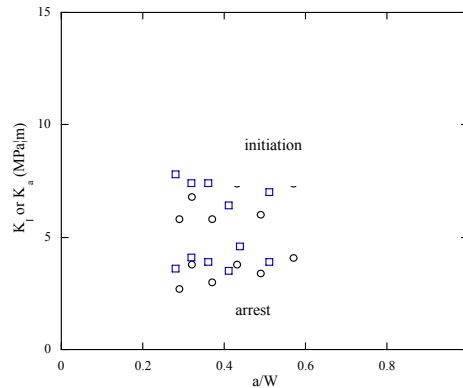


Fig. 10. The final TiAl calibration data showing consistent scatter bands of K_{Ic} (upper) and K_{Ia} (lower) toughness values.

Summary Discussion and Concluding Remarks

A chevron notched, wedge loaded double cantilever beam (CWB) test method to measure the initiation and arrest fracture toughness of brittle and semi-brittle materials using very small composite specimens and that can be fabricated using minimal amounts of critical materials has been developed. This report focuses on finite element (FE) simulations that were used to select a specimen geometry that is effective, and to quantify the stress intensity factor (SIF) for the CWB specimen. An effective geometry to facilitate initiation and arrest events was found to be a thickness ratio, $W/B = 2$, a height to thickness, $h/B = 0.5$, and an initial crack depth to width ratio, $a_o/W = 0$. The SIF for this geometry decreases rapidly with increasing a/W between 0 to 1. Combined with the wedge loading, this configuration results in stable crack growth, manifested as a series of short pop-in events. The FE solutions provide the basis to evaluate K_{Ic} and K_{Ia} for a specified CWB specimen size (B), the elastic modulus (or moduli) of the fixture and specimen material(s) (E), the critical crack mouth (load line) displacement (Δ_c) and the crack depths (a_i/W and a_a/W) at initiation and arrest.

Notably, the SIF varied by approximately 30% along the crack front between a broad minimum at the center and a local maximum at the chevron edges. Thus we believe proper analysis of CWB data requires the use of two SIF versus a/W curves. The curve for the edge specifies the $K_I = K_{Ic}$ at initiation, while the curve for the center specifies the $K_I = K_{Ia}$ at arrest. The variation in the SIF is larger if the crack front is slanted. In this case, the SIF is highest where the crack front forms an acute angle with the side of the chevron and lowest where it forms an obtuse angle with the chevron side. However, the maximum SIF is only slightly higher than that for an unslanted crack front, while the minimum is about 10-20% lower than for the corresponding SIF at the middle of an unslanted crack. Since the fracture may initiate at a one point, but must arrest over an appreciable length of crack front, use of the SIF functions for unslanted cracks to evaluate K_{Ic} and K_{Ia} from CWB tests is a reasonable approximation.

Plastic deformation reduces the SIF relative to a fully elastic condition. The effect plasticity depends on a/W , and is modest below about $0.01\Delta/B$ for $a/W = 0.2$ and $0.025\Delta/B$ for $a/W = 0.5$. This assessment is based only on continuum elastic loading criteria and does not account for difference in the local crack tip fields due to a variety of factors, ranging from T-fields effects, to detailed variations in local deformation patterns.

Tests on cleavage oriented iron single crystals were carried out on composite sandwich specimens, with thin (t) crystal slices diffusion bonded to low alloy steel arms. The FE simulations were used to assess the corresponding interfaces stresses as a function t . A thickness of $t = 1$ mm was found to be sufficient to avoid high normal interface stresses that could lead to debonding. The effects of elastic modulus differences on the SIF between the single crystal Fe and the steel arms were also evaluated; while this effect was minimal, the sandwich SIF as function of a/W was used in the Fe single crystal K_{Ic} and K_{Ia} evaluations.

Implementation of the CWB test method was carried out on a precision-machined wedge loading crack mouth opening displacement fixture, driven by a MTS servohydraulic load frame. The test was instrumented with a clip gauge to measure Δ . The CWB method was evaluated by testing TiAl specimens, with previously reported $K_{Ip} \approx 7.1 \pm 0.7$ to $K_{Ic} \approx 8 \pm 1$ $\text{MPa}\sqrt{\text{m}}$, for a notched CAB and fatigue precracked three point bend specimens, respectively. The CWB tests, including the scoping studies with a simpler loading device, gave a corresponding average $K_{Ic} \approx 7.1 \pm 1$ $\text{MPa}\sqrt{\text{m}}$, in good to excellent agreement with the previous results. The average K_{Ia} for the CWB tests on TiAl was 3.7 $\text{MPa}\sqrt{\text{m}}$, compared to an average of 2.8 ± 1.4 $\text{MPa}\sqrt{\text{m}}$ measured by the CAB tests.

Static CWB tests at -196°C gave an average of $K_{Ic} = 11.4 \pm 3.8$. This compares well with a corresponding value of 12.5 ± 2.7 $\text{MPa}\sqrt{\text{m}}$ measured by CAB tests, but is much higher than the 5.8 ± 0.6 $\text{MPa}\sqrt{\text{m}}$ measured in static sharp pop-in crack 4-point bend tests. This difference may be partly due to the fact that the CWB tests are conducted at a slightly lower effective loading rate than the static 4-point bend tests. However as noted in a companion report [7], the K_{Ic} from the CAB tests are believed to be overestimates of the actual initiation toughness for a variety of reasons. Further, initiation may not always be exactly at the chevron-crack front corner. Thus it is recommended that the lower grouping of the CWB data be averaged to estimate the actual K_{Ic} , with a minimum of at least 2-4 data points. Alternately the highest, or few highest, K_{Ic} data point(s) could be eliminated in the averaging, especially if they differ appreciably from the other data. The former method gave an average K_{Ic} of $8.55 \pm$ $\text{MPa}\sqrt{\text{m}}$ for the iron single crystals, which is more consistent with the 4-point bend test data extrapolated to the lower loading rates.

In summary, CWB tests on polycrystalline TiAl and Fe single crystals were successfully carried out using small specimens with dimensions of $8 \times 4 \times 4$ mm. Thus the CWB test method offers a powerful new tool to measure the fracture toughness of brittle and semi-brittle materials, especially when specimen sizes and or the availability of materials are an issue.

Future Work

The CAB and CWB test methods have been used to very successfully characterize the K_{Ia} in cleavage oriented iron single crystals, between -196 and 0°C [5]. The resulting database is unique and has, for the first time, clarified the fundamental dynamics and controlling mechanisms of cleavage fracture. This database has also been used to develop a preliminary, but powerful, new semi-empirical multi-scale model of the macroscopic $K_{Ic}(T)$ curve for complex structural steels. Notably, this model predicts an approximately invariant shape of the master toughness-temperature curve for complex steels, as well as the reference temperature shifts in the master curve due to irradiation hardening, that are in agreement with observation. Further analysis of the database and development of the model as well as full documentation of these results, including preparation of manuscripts for journal publication, will be completed during this current reporting period.

References

- [1] ASTM Standard E 1304-97, Standard Test Method for Plane-Strain (Chevron Notch) Fracture Toughness of Metallic Materials, V03.01 (2006) 914.
- [2] M. Y. He and A. G. Evans, Three-dimensional Finite Element Analysis of Chevron-Notched, Three-Point and Four-Point Bend Specimens, Fracture Mechanics: Twenty-Second Symposium V1, ASTM STP 1131 (1992) 471.
- [3] R. J. Hartranft and G. C. Sih, An approximate 3-dimensional theory of plates with application to crack problems, Int. J. Eng. Science 8 (1970) 711.
- [4] N. P. O'Dowd and C. F. Shih, Two-parameter Fracture Mechanics: Theory and Applications, Fracture Mechanics: Twenty-Fourth Volume, ASTM STP 1207 (1994) 21.
- [5] M. L. Hribernik, Cleavage oriented iron single crystal fracture toughness, Ph.D. thesis, University of California, Santa Barbara, 2006.
- [6] G. R. Odette, B. L. Chao, J. W. Sheckherd, and G. E. Lucas, Ductile phase toughening mechanisms in a TiAl-TiNb laminate composite, Acta Metall. Mater. 40 (1992) 2381.
- [7] M. Y. He, G. R. Odette, and M. L. Hribernik, A compression anvil beam test method to measure the arrest fracture toughness of semi-brittle materials with small specimens, Fusion Materials Semiannual Progress Report for the Period Ending June 30, 2007, DOE-ER-0313/42.